3D Photoacoustic Tomography Setup Calibration

Sumith K K

A dissertation submitted for the partial fulfillment of BS-MS dual degree in Science

Department of Physical Sciences
Indian Institute of Science Education and Research
Mohali

June 2020

Certificate of Examination

This is to certify that the dissertation titled "**3D Photoacoustic Tomography Setup Calibration**" submitted by Sumith K K (Reg. No. MS15171) for the partial fulfillment of BS-MS dual degree programme of the institute, has been examined by the thesis committee duly appointed by the institute. The committee finds the work done by the candidate satisfactory and recommends that the report be accepted.

Dr. Ananth Venkatesan Dr. Sanjib Dey Dr. Samir Kumar Biswas
(Supervisor)

Dated: June 15, 2020

Declaration

The work presented in this dissertation has been carried out by me under guidance of Dr. Samir Kumar Biswas at the Indian Institute of Science Education and Research Mohali.

This work has not been submitted in part or in full for a degree, a diploma, or a fellowship to any other university or institute. Whenever contributions of others are involved, every effort is made to indicate this clearly, with due acknowledgement of collaborative research and discussions. This thesis is a bonafide record of original work done by me and all sources listed within have detailed in the bibliography.

Sumith K K
(Candidate)

Dated: June 15, 2020

In my capacity as the supervisor of the candidate's project work, I certify that the above statements by the candidate are true to the best of my knowledge.

Dr. Samir Kumar Biswas
(Supervisor)

Acknowledgements

For the most part, I would like to express my gratitude to Dr. Samir Kumar Biswas, for his mentorship throughout this research. It's been a great experience to have him learn from him as a supervisor and mentor.

I would like to thank Dr. Ananth Venkatesan and Dr. Sanjib Dey , the members of my thesis committee for the discussions and suggestions during the presentations which helped me shape my research further.

My heartfelt thanks go to Dr.Sriram Krishnan for helpful discussion of the projects.I want to thank all my fellow lab mates at Bio-Nano-Photonics lab: Nitin Burman, Sanjay Kapoor, Laxman Das, Amit Yogi, Aniket L Chavan,Bhal Singh,Dr. Gurpreet Kaur for helping me whenever needed.

Also, I want to thank my friends Nihal Muhammed, Vishnu KP, and Asif Mohammed for the sleepless nights that we worked together before the weekly presentation.

I want to express my gratitude to my parents for their support, and freedom. Also I thank my friends Sandra Sajan, Fidha Nazrin, Athul Viay, Alan Babu, Balashankar , Akshay Menon,Gokul and Nikhil Sivakumar.

List of Figures

Contents

Dedicated to my father.

Abstract

Photoacoustic tomography is a fast-growing biomedical imaging method for last few years.In photoacoustic tomography, the target is illuminated by a pulsed laser and the absorption of the light leads to an outward travelling pressure wave called a photoacoustic effect. This pressure wave is used for image reconstruction of the optically illuminated object. Domain for the PAT is both optical and acoustic so that it has a lot of advantages as high penetration depth, good spatial resolution, high contrast, etc. Because of its non-ionising property it is widely using in medical field related to micro-vascular systems.

This thesis is about the calibration of 3D photoacoustic setup. The calibration is aims to find the geometrical parameters which are needed for image reconstruction. For the calibration a detector array is rotating around the calibration object and estimates the calibration parameters which are speed of sound, source position, the center of rotation of detector array.

Chapter 1

Introduction

1.1 The photoacoustic effect

Photoacoustic effect is the formation of acoustic energy from absorption of optical energy in an object. The thermoelastic expansion of the target area leads to the generation of the ultrasound.When the laser pulses are delivered to the target area, the absorbed energy leads to the heating of the tissue part, which causes transient thermoelastic expansion. When the pulsed laser is off, the expanded tissue contracts will generate outward traveling pressure waves [Hoelen 98]. The laser heating has two crucial time scales, thermal and stress relaxation time[Wang 12]. The attribute of thermal diffusion carried out by the thermal relaxation time and it is given by :

$$\tau_{th} = \frac{d^2}{\alpha} \tag{1.1}$$

Where α is the thermal diffusivity. Stress relaxation time is involved with the attributes of pressure propagation and which is estimated by

$$\tau_s = \frac{d^2}{c} \tag{1.2}$$

In order to get better result the laser has to satisfy thermal confinement and stress confinement conditions[Willemink 10].The condition when pulse width is less than the thermal relaxation time, called thermal confinement.Likewise, if the laser pulse width is less then stress relaxation time called stress confinement. Thermal confinement

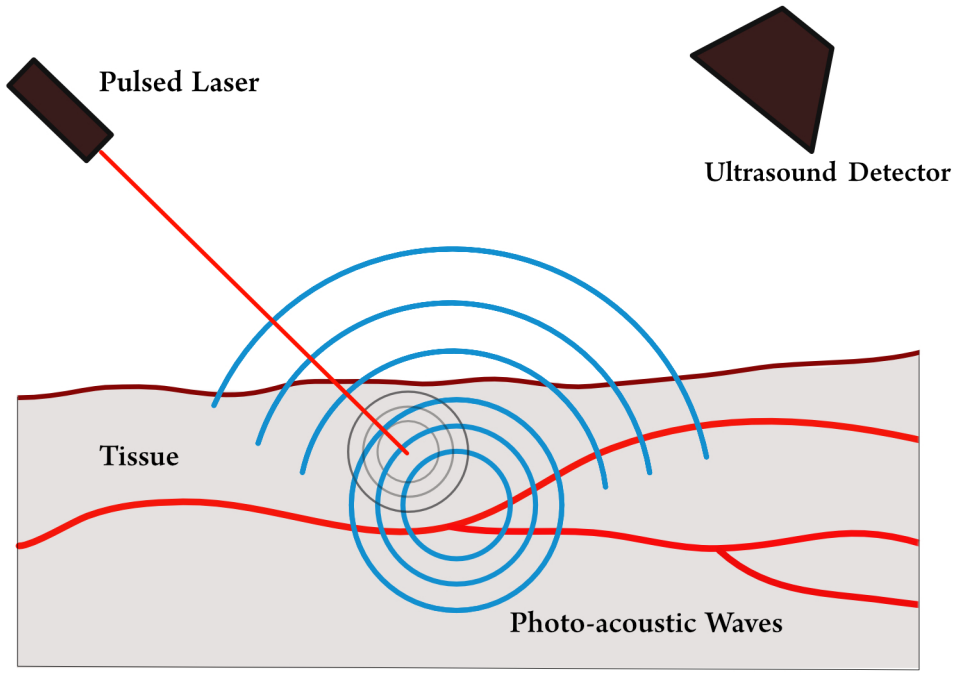

FIGURE 1.1: Photoacoustic effect

conditions depending on the heat diffusion in the material, and the stress confinement is on the pressure propagation.

The heating of an object is represented by a space-time function $H(r,t)$. Let the temperature distribution is $T(r,t)$, and then the temperature rise will be :

$$\rho C_p \frac{\partial T(r,t)}{\partial t} = \lambda \nabla^2 T(r,t) + H(r,t) \tag{1.3}$$

In thermal confinement conditions the heat equation reduces to (1.4).Where C_p is specific heat,ρ is the density, β is the volume expansion coefficient, and λ is thermal conductivity[Francis 16].

$$\rho C_p \frac{\partial T(r,t)}{\partial t} \approx H(r,t) \tag{1.4}$$

The wave equation gives the relation between temperature distribution and acoustic pressure:

$$\nabla^2 p(r,t) = \frac{1}{c^2}\frac{\partial^2}{\partial t^2}p(r,t) - \beta\rho\frac{\partial^2}{\partial t^2}T(r,t) \tag{1.5}$$

Under thermal confinement conditions :

$$\nabla^2 p(r,t) = \frac{1}{c^2}\frac{\partial^2}{\partial t^2}p(r,t) - \frac{\beta}{C_P}\frac{\partial}{\partial t}H(r,t) \tag{1.6}$$

The laser pulse will be considered as a delta function in stress confinement conditions. The initial pressure at t = 0 is $\frac{\beta c^2}{C_p}A(r)$ Then the pressure equation in terms of initial pressure is :

$$p(r,t) = \frac{1}{4\pi c^2}\frac{\partial}{\partial t}\left\{\frac{1}{ct}\iint dr' p_0(r')\Big(t - \frac{|r-r'|}{c}\Big)\right\} \tag{1.7}$$

This model ignored the acoustic attenuation and considered a constant speed of sound in calibration object.

1.2 Scope and context

Alexander Graham Bell discovered the photoacoustic effect in 1880 . But its use in the medical field began only recently after the invention of the ultrasound transducers[Wang 08, Ku 01, Kostli 01, Xu 02, Köstli 03, Ku 04]. In photoacoustic tomography, both acoustic and optical properties have influences, which leads to good results in the imaging [Xu 06]. Pure optical imaging methods are also there where the analysis is done by the intensity variations, but its sensitivity is weak when compared to photoacoustic imaging. Ultrasound in soft tissues has less scattering, ensuring that it can travel longer distances, which provides the imaging of deeper tissues[Kruger 95]. Different shapes of ultrasound transducers available for photoacoustic imaging[Kolkman 08, Minghua Xu 02, Zemp 07, Manohar 04, Vaithilingam 09], and we've chosen a linear detector array setup where the imaging object is stationary, and the detector array rotates around the object.

Measurements

To do three-dimensional imaging of an object, we have to perform calibration measurement of the setup to estimate calibration parameters. The calibration has to be done using the calibration object with point sources. A schematic overview of the calibration measurement and object measurement is shown below.

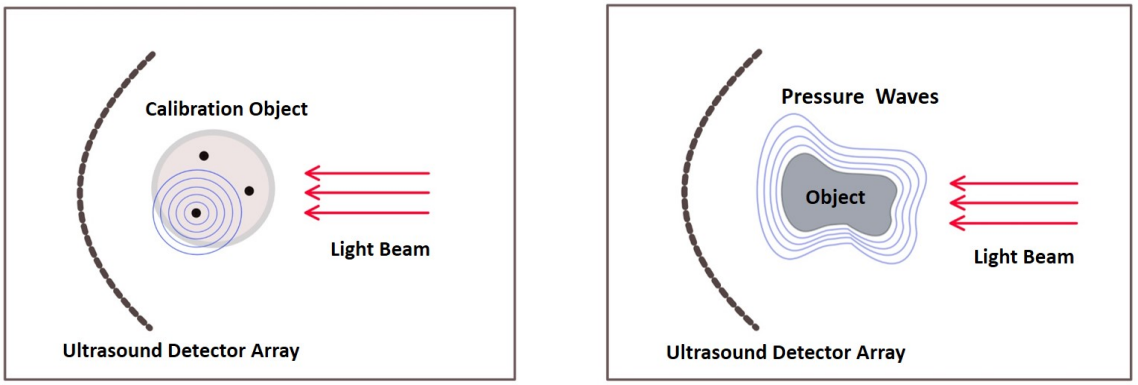

(A) Calibration measurement (B) Object measurement

FIGURE 1.2: Schematic representation of the calibration measurement

Calibration is very crucial in this 3D photoacoustic tomography, because of the geometrical parameters are necessary for the image reconstruction [Willemink 10]. It is difficult to fix the center of rotation at pre-assigned coordinates. Also, it isn't easy to align the linear detectors straight and exactly parallel to the axis of rotation.

Chapter 2

Calibration Setup

2.1 Introduction

This chapter outlines an algorithm, which is necessary for proper image reconstruction. The calibration algorithm is used to calibrate the geometrical shapes of the setup used for the measurement. This chapter describes the algorithm, which split into small parts and concludes with a robust algorithm that calibrates the whole measurement setup.

2.2 Calibration Parameters

There are two types of parameters that are included in our calibration parameters, Internal and External parameters. The parameters which are related to the measurement array are called internal parameters, and others are called external parameters. We assume that internal parameters remain fixed, and the external parameters can change in between the measurement session; however, it remains fixed during a single measurement.

Internal Parameters : Length of the linear array (l) , Radius of the curved array (r), Position of the i^{th} sensor element ($p_{d,i}$), Spacing between sensor elements (d)

External Parameters : Center of rotation (T), Position of the photoacoustic point source (P_s), Speed of sound (c)

2.3 Measurement array setup

There are three kinds of measurement array geometry we have to discuss in this section. In two-dimensional, a linear detector with 128 sensor elements and curved detector with 128 sensor elements. In the three-dimensional,a linear detector with 128 sensor elements which is parallel to the axis of rotation. A schematic overview of both two-dimensional measurement array geometry is shown below.

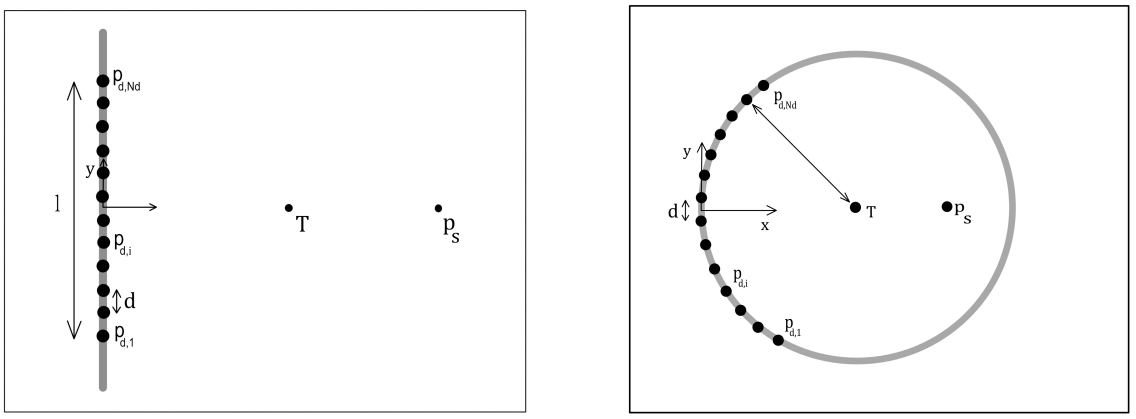

(A) Linear detectory (B) Curved detector

FIGURE 2.1: Two-dimensional measurement array setup. In both geometries, the detector elements are depicted using black dots denoted labelled $P_{d,i}$. The spacing between the detector elements is indicated by d. The photoacoustic point source is near the center of rotation and labeled by P_s. The length of the arrays is labeled with l and the radius with r .

For the detector element positions, we are setting the middle of the measurement array as origin. The detector array contains N_d elements and distance between each elements is d.

In the curved sensor array radius of curvature is r and the position of detector elements is given by Equation 2.1

$$p_{d,i} = r \begin{bmatrix} 1 - \cos\left((i - \frac{N_d+1}{2})\frac{d}{r}\right) \\ \sin((i - \frac{N_d+1}{2})\frac{d}{r}) \end{bmatrix} \tag{2.1}$$

For the linear measurement array, we have to consider the curved array with a radius of curvature tends to infinity :

$$p_{d,i} = \lim_{r\to\infty} r \begin{bmatrix} 1-\cos\left((i-\frac{N_d+1}{2})\frac{d}{r}\right) \\ \sin((i-\frac{N_d+1}{2})\frac{d}{r}) \end{bmatrix} = \begin{bmatrix} 0 \\ (i-\frac{N_d+1}{2})d \end{bmatrix} \tag{2.2}$$

In three dimensional geometry, we have used a linear measurement array parallel to the z-axis is shown in the Figure 2.2. The linear detector array is confined to a cylindrical shape, and we placed the sources at the central part of the cylindrical shape so that the detector array could measure different angles of the cylindrical shape. So we have to introduce new parameters, rotation angle ϕ, and the radius of the cylindrical shape r_1.The position of detector elements in the 3D model is given by Equation 2.3

$$p_{d,i} = \begin{bmatrix} r\cos\phi \\ r\sin\phi \\ (i-\frac{N_d+1}{2})d \end{bmatrix} \tag{2.3}$$

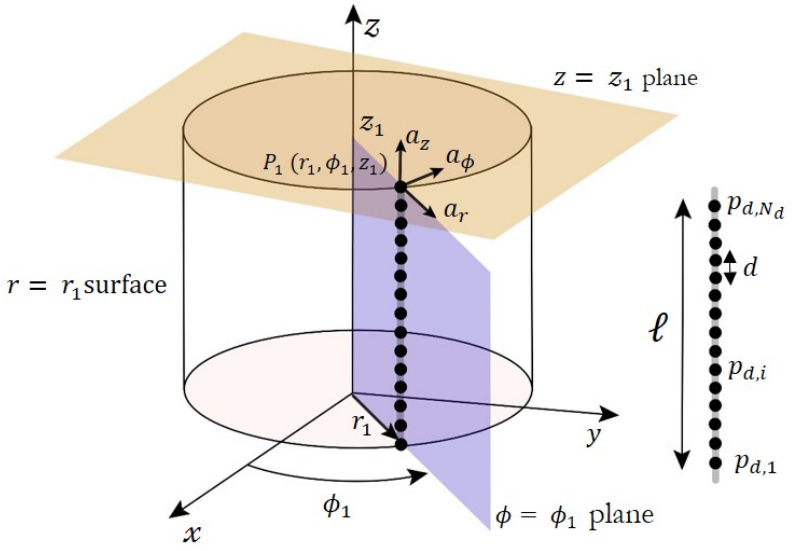

FIGURE 2.2: Schematic of the three-dimensional measurement array geometry. The detector elements are depicted using black dots, and its position is denoted by $P_{d,i}$, and the distance between the detector elements is indicated by d.The linear detector array is confined to a cylindrical shape with centerline as the z-axis. The center of rotation will be the middle of the centerline which is labeled by T. The radius of the cylinder is labeled r_1, and the rotation angle is labeled by ϕ

2.4 Calibration measurement model

Calibration measurement aims to find the parameters, speed of ultrasound (SOS) of the calibration object and center of rotation . The basic structure of the calibration setup is the 3D measurement array, which rotates step wise around the calibration object. The measurement array records flight time at each step, and this time of flight data is used to find the calibration parameters.

To make the estimation simple, we assume that speed of ultrasound in calibration object and reference medium are equal. Consider a measurement array of N_d detector elements, N_R rotation steps and N_p point sources in the calibration object, we will have $N_R \times N_p \times N_d$ total number of times of flight data.. Then the measurement function will be:

$$z_{tof,i,j,k} = \frac{1}{c}\|p_{d,i} - (R_{\phi j}p_{s,k} + T)\| + n_z \tag{2.4}$$

Where i, j and k are the indexes of detector elements, rotation steps, and point sources respectively and n_z is the additive noise. The complete measurement function is given by:

$$h_{tof}(c, T, p_{s,1}, \ldots, p_{s,N_p}) = \left(\left(\left(h_{tof}(c, T, p_{s,1}, \ldots, p_{s,N_p})\right)_{i=1}^{N_d}\right)_{j=1}^{N_R}\right)_{k=1}^{N_p} \tag{2.5}$$

as provided by [Willemink 10].

2.5 Construction of 3D model

The three-dimensional calibration setup was simulated using a Matlab toolbox called 'k-wave'[Treeby 10]. In 3D model construction, generated point sources for the generation of acoustic waves and detector array for the detection of generated acoustic waves. The point source in k-wave generates the pressure waves which is similar to the pressure waves of a pulsed laser exposing to a photoacoustic material. The propagating medium properties also included so that the pressure wave matches the actual waves.

The k-wave toolbox simulates the detector element as a position and it would give the pressure wave at that position, which would be the pressure wave amplitude if we placed an ultrasound detector in the same position. As explained in the measurement array geometry section, a linear array of 128 pseudo ultrasound detectors are arranged in a linear array which is parallel to the axis of rotation. The detector we are used in this k-wave toolbox is called pseudo ultrasound detector because measures the amplitude of the propagating pressure wave. The linear detector array is confined to a cylindrical shape and we placed the sources at the central part of the cylindrical shape so that the detector array could measure different angles of the cylindrical shape. This each measurement at different angles called projections. The simulated 3D model is shown in Figure 2.3a.

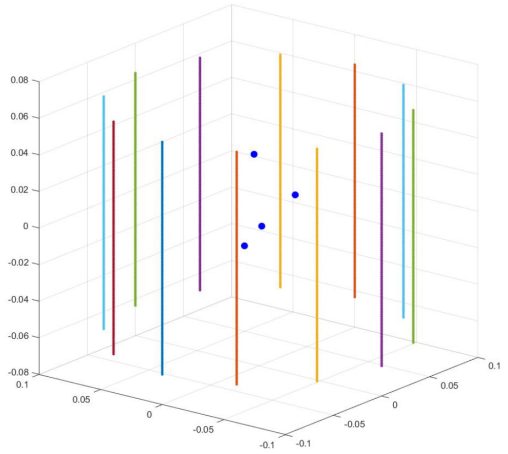

(A) Detector array is parallel to z-axis

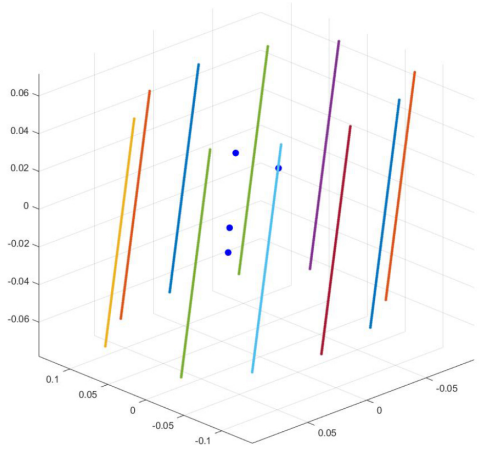

(B) Detector array with slight inclination

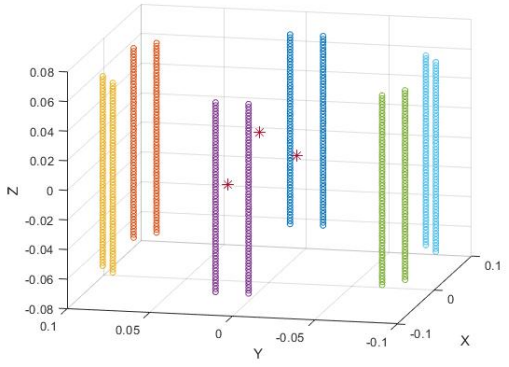

(C) Simulated three-dimensional model of combined two projections

FIGURE 2.3: Simulated three-dimensional models

Practically it is very difficult to align the detector array exactly parallel to the axis of rotation. So inclination introduced in the 3D model detector array. The model is shown in the Figure 2.3b. The calibration measurement was done using another measurement array geometry where we combined two projections as a single projection. The combined projection model is shown in Figure 2.3c. This setup is more convenient for better calibration and image reconstruction which will explain in the calibration algorithm section.

Chapter 3

Calibration Algorithm

3.1 Time of flight estimation

The extraction of flight data time is the first step of the calibration process. Flight time (TOF) is the time that the generated ultrasound takes to reach the elements of the detector array. The measured signal is the time-shifted and amplitude modulated source signal with additional noises. For the calibration purpose, we are using the k-wave generated ultrasound signals, but in the experiment, we are creating the ultrasound using optical absorber. The shape of the ultrasound depends on the object ,and it can change in between the different calibration measurements. So simultaneously, we try to estimate ultrasound signal, time of flight, and the amplification or attenuation factors. We cannot find a unique solution to the problem. To get rid of the problem, we are constraining the phase by enforcing the center of mass(COM) to the middle of the signal window[Willemink 10]. The constraint is given as:

$$\int_{t=t_1}^{t_2} t \frac{h_{env}(t)}{\int_{t'=t_1}^{t_2} h_{env}(t')dt'} dt = \frac{t_1 + t_2}{2} \tag{3.1}$$

Where h_{env} is the magnitude of the signal called the envelope of the signal given in Equation 3.2 and $\mathcal{H}\{h(t)\}$is the Hilbert transform of the signal.

$$h_{env}(t) = \sqrt{h^2 + (\mathcal{H}\{h\})^2} \tag{3.2}$$

The amplitude is constrained by implementing the utmost of the signal to be one. The different steps in the algorithm for estimating time of flight and source signal are explained further.

- **Step 1: Initialization** A window of a measured signal which approximately covers the source signal as taken as the initial estimate of the source signal.
- **Step 2: Applying the source signal constraints** In this step, we applied the source signal constraints, which we discussed earlier. First, as shown in the Equation 3.2, the signal envelope is calculated, and then COM of the signal is calculated using Equation 3.1. Then source signal will shift according to the dissimilarity between the center of the signal window and the measured center of mass.
- **Step 3: Time of flight estimation step** Using the calculable source signal simply, we are able to estimate the time of flight and therefore the attenuation or amplification factors.. It is a template-based approach, where we compare the estimated source template with the actual source signal and the time shift will be the time of flight. We estimate the time of flight for each measured signal.
- **Step 4: Source signal estimation step** The source signal is estimated by rearranging the signals with the calculated time of flight. The weighting factors for likelihood estimation are calculated from the amplification or attenuation factors. The result of the step is used for the next iteration, where we apply the source signal constraints.

The output of the time of flight estimation is given in Figure 3.1a and k-wave generated the raw data is shown in Figure 3.1b.

3.2 Time of flight classification

Grouping the TOF measures is a necessary step because, if more than one point sources present in the phantom, we cannot directly fit the data for the calibration parameters. Even though the user can define the number of sources for the calibration

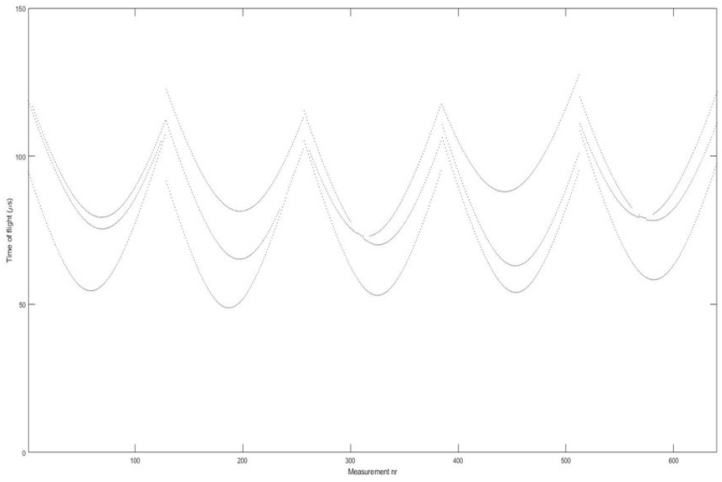

(A) Calculated TOF data

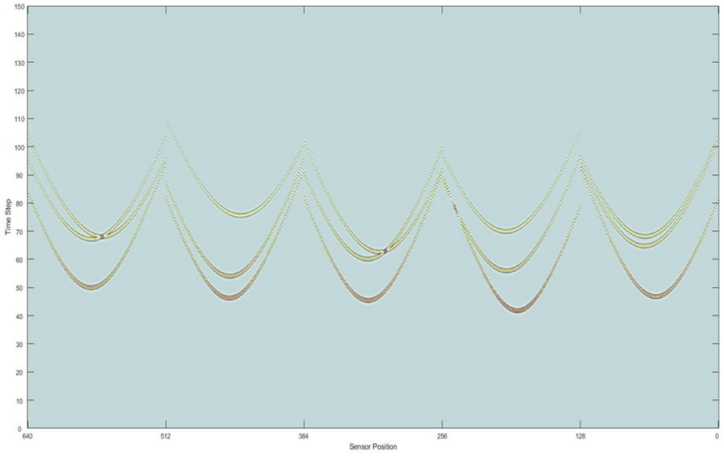

(B) Raw TOF data

FIGURE 3.1: Estimated and raw TOF data

measurement, the grouping algorithm has to find the number of sources and classify each time of flight data into any of the classes (source) or to the outliers. Outliers are the false measurements recorded by the detectors. Accuracy of the calibration increases with the number of the point sources. We have to design a versatile algorithm so that it classifies each time of flight data into any of the classes without the information of the user-defined number of sources.

Before going to the grouping, we will discuss about the estimated TOF data. In the Figure 3.2, showed the estimated time of flight data with vertical lines separates each projections. The time of flight data corresponding to each source can be fitted using a second-order polynomial. The number of polynomials in each rotation is the

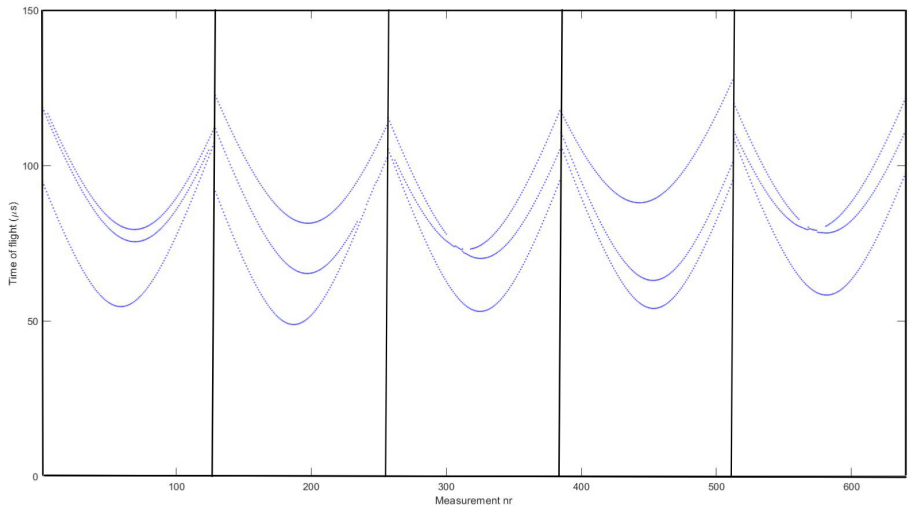

FIGURE 3.2: Example of a Time of flight data using 128 element linear sensor array($N_d = 128$), over five different angles($N_R = 5$) and three point sources(N_p=3).Each projection is separated by vertical lines.

number of sources. Still, it need not be the actual number of sources because it is not necessary to see all the sources in every rotation. We expect there is some deviation in the measurement from the polynomial model, so we have introduced Gaussian error with zero mean and standard deviation σ_z. We already mentioned the aim of this classification, but the classification step is to proceed with each rotation separately. It leads to another problem, the correspondence of sources in each rotation, and we postponed this problem to another step. The classification step is based on using the mixture models[McLachlan 88]. It estimates the probability that each data belongs to a specific group (Either any of the sources or outliers).

Let's consider the time of flight data with N measurements,$z = [z_1, \ldots, z_N]$. The i^{th} measurement was measured by the sensor element s_i, and it is caused by the k^{th} source and the polynomial parameter x_k then we have:

$$z_i = h_i(\mathbf{x}_k) + n_{i,k} \tag{3.3}$$

where the polynomial function $h_i(x_k)$ is the time of flight prediction function with independent variable as sensor number:

$$h_i(x_k) = x_{k,1}s_i^2 + x_{k,2}s_i + x_{k,3} \tag{3.4}$$

The Gaussian random variable with standard deviation σ_z is the noise, and it is represented by $n_{i,k}$ for the i_{th} measurement.We have to introduce a membership variable to describe the relationship between the measurement and the source number,$\gamma = [\gamma_1, \ldots, \gamma_N]^T$ where each entry represents the i^{th} measurement and the γ_i is the class number. Then we have the relation :

$$z_i = \sum_{k=1}^{N_s} I_k(\gamma_i)\big(h_i(X_k) + n_k\big) + I_0(\gamma_i)n_0 \tag{3.5}$$

where the Indicator function $I_k(\gamma_i)$:

$$I_k(\gamma_i) = \begin{cases} 1 & \gamma_i = k \\ 0 & \gamma_i \neq k \end{cases} \tag{3.6}$$

Based on these relations, the likelihood function is given as :

$$p(z_i|\chi, \gamma_i) = \sum_{k=1}^{N_s} I_k(\gamma_i) \frac{1}{\sqrt{2\pi}\sigma_z} e^{-\frac{1}{2}\frac{r_i^2(X_k)}{\sigma_z^2}} + I_0(\gamma_i)\frac{1}{v} \tag{3.7}$$

Where $\chi = (X_1, \ldots, X_{N_s})$ is the polynomial parameters and $v = z_{max} - z_{min}$ is the range of time of flight domain and $r_i = h_i(x) - z_i$ is the residue of the i^{th} measurement.The combined likelihood function of all the measurement is given in Equation 3.8 which the product of all the individual likelihood functions:

$$p(z|\chi, \gamma) = \prod_{i=1}^{N} p(z_i|\chi, \gamma_i) \tag{3.8}$$

By maximizing the likelihood function, we could get the polynomial parameters and assign each measurement to any of the groups[Fletcher 13]. There is a possibility of the measurement at the intersection can be originated from either one of the classes. Also, measurement can fully assign to any of the sources or outliers. To get rid of this problem, we split the likelihood maximization into two steps, first maximize with X independent on membership variable then find the probability of each measurement to any of the classes. The individual marginalized likelihood function (Independent of gamma) is given as:

$$p(z_i|\chi) = \frac{1}{(N_s+1)\sqrt{2\pi}\sigma_z}\left(\sum_{k=1}^{N_s} e^{-\frac{1}{2}\frac{r_i^2(X_k)}{\sigma_z^2}} + \frac{\sqrt{2\pi}\sigma_z}{v}\right) \tag{3.9}$$

Probability of a measurement belongs to any of the source group ($k > 0$) :

$$p(\gamma_i = k|z_i, \hat{\chi}) = \frac{e^{-\frac{1}{2}\frac{r_i^2(X_k)}{\sigma_z^2}}}{\sum_{k'=1}^{N_s} e^{-\frac{1}{2}\frac{r_i^2(X_{k'})}{\sigma_z^2}} + \frac{\sqrt{2\pi}\sigma_z}{v}} \tag{3.10}$$

and the probability of certain measurement to be an outlier is given by:

$$p(\gamma_i = 0|z_i, \hat{\chi}) = \frac{\frac{\sqrt{2\pi}\sigma_z}{w}}{\sum_{k'=1}^{N_s} e^{-\frac{1}{2}\frac{r_i^2(X_{k'})}{\sigma_z^2}} + \frac{\sqrt{2\pi}\sigma_z}{v}} \tag{3.11}$$

Instead of maximize the likelihood function, we use the concept of cost function which is the negative logarithmic of likelihood. Here, the cost function will be the sum of all the individual cost functions. The cost function minimization faces the problems of local minima, also the number of groups is an unknown parameter. SO we used an algorithm called RANSAC(Random sampling consensus) [Fischler 81]. RANSAC algorithm is used for the strong work of model parameters once outliers are present in the data. The technique RANSAC minimize the cost is based on randomly selecting large number of small subsets from observed data. The RANSAC cost function is given by :

$$\rho_{RANSAC}(r) = \begin{cases} 0 & \frac{r^2}{\sigma_z^2} \leq T \\ 1 & \frac{r^2}{\sigma_z^2} > T \end{cases} \tag{3.12}$$

Where threshold T decides measurement belongs to which group inliers or outliers. The size of the random sampling subset in RANSAC is chosen as the smallest number enough to fit the model and denoted by $N_{s,min}$. Let the sample is $S = (i_1, \ldots, i_{N_{s,min}})$; we use this subset to fit the model and obtain the residue of all the measurements according to the fitted parameters. This resultant residue decides each measurement belongs to an inlier or outlier. This method will do over all the sampled set for many

trials, and the final inlier set can be used for the parameter fitting using least-squares optimization. The minimum number of trials required to ensure a probability ϵ :

$$\hat{N}_{trials} = \left\lceil \frac{log(1-\epsilon)}{log\left(1-\left(\frac{N_{target}}{\hat{N}_0}\right)^{N_{s,min}}\right)} \right\rceil \tag{3.13}$$

Where N_{target} is the number of measurement belongs to the new class and $N_{s,min}$ is the smallest subset size number enough to fit the model. Here the size of the subset $N_{s,min} = 3$, because to fit a second-order polynomial we need a minimum of three data points $S = (i_1, i_2, i_3)$. The subset elements should be from different sensor elements. The fitted parameter is:

$$\mathbf{x} = \mathbf{H}_S^{-1}\mathbf{z}_S \quad \text{with} \quad \mathbf{H}_S = \begin{bmatrix} s_{i_1}^2 & s_{i_1} & 1 \\ s_{i_2}^2 & s_{i_2} & 1 \\ s_{i_3}^2 & s_{i_3} & 1 \end{bmatrix} \tag{3.14}$$

An example of a grouping result of the time of flight of three sources over five projections is shown in Figure 3.3. We already mentioned the measurement array setup used for this thesis is a combined projection of two linear detector arrays, and the configuration is shown in Figure 2.3c. The time of flight data from the combined projection setup is shown in Figure 3.4.

We propose a post-grouping step to make sure of the correspondence of each source of two separate projections. We execute pairs from two linear projection of a combined projection based on the least deviation among all the time of flight data. The pairwise grouping of the first projection is displayed in Figure 3.5.

3.3 Estimation of source position and speed of sound

The TOF classification step estimated the number of sources in the measurement setup and the probability of each measurement into the source group.From this grouped time of flight data, we will estimate source position and speed of sound.To accomplish this, in the measurement model, we used phantom with some sources. The optimization

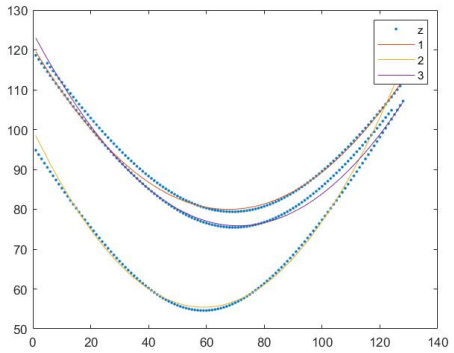

(A) Measurement 1 ($\phi = 0°$)

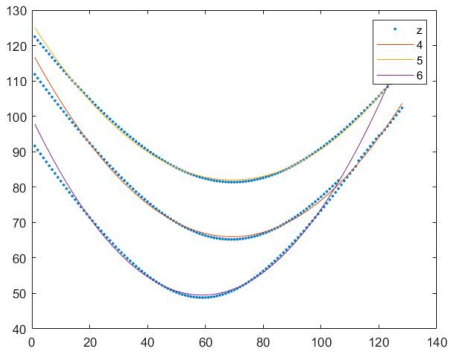

(B) Measurement 2 ($\phi = 72°$)

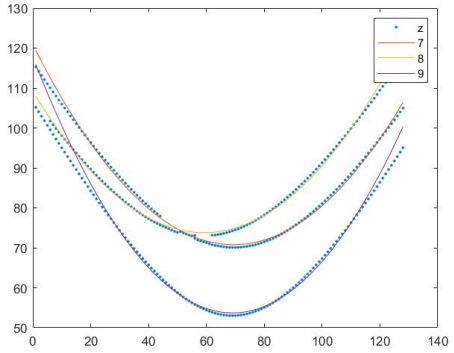

(C) Measurement 3 ($\phi = 144°$)

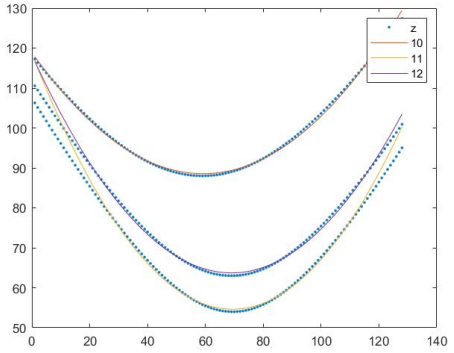

(D) Measurement 4 ($\phi = 216°$)

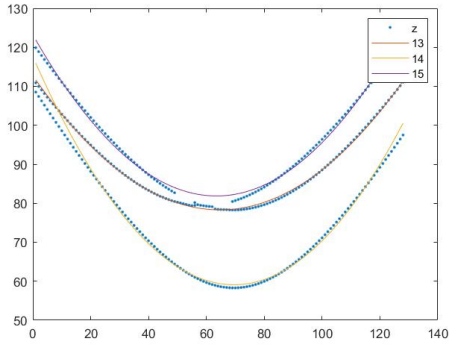

(E) Measurement 5 ($\phi = 288°$)

FIGURE 3.3: TOF classification result.

is complicated when we estimate all the parameters together because of the presence of local minima. The source position estimation step is to proceed with a different method. We try to predict the source position separately in each projections called relative source position. The time of flight classification was solved all rotations $R \in \{1\ldots, N_R\}$ individually, and the sources in each rotation is labeled by $\hat{N}_{s,R}$ and second order polynomial parameters are $\hat{\chi}_R = (\hat{x_1}, \ldots, \hat{x}_{N_s,R})$. We combine all

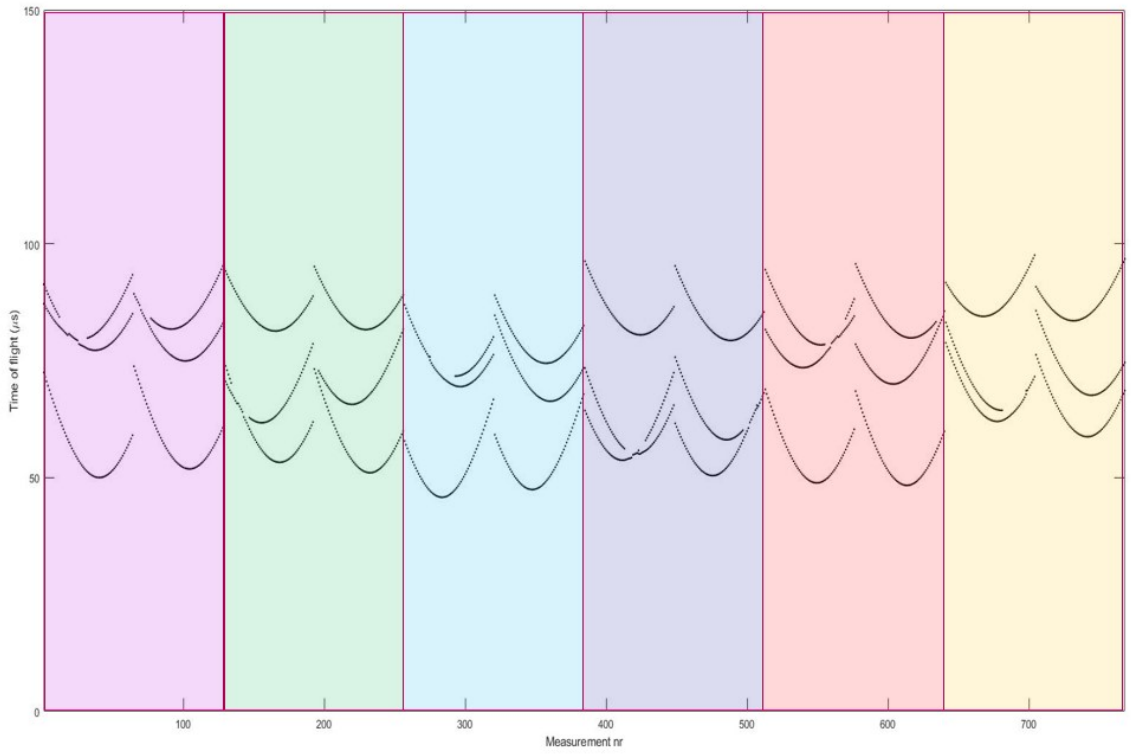

FIGURE 3.4: Example of combined projection time of flight data. Different combined projections is separated by vertical lines.Linear sensor array of 64 sensor elements ($N_d = 64$), over six different angles($N_R = 6$) and three point sources($N_p = 3$)

the measurements overall projections to estimates the speed of sound and source positions. When we are dealing with relative source positions, we have to introduce an indicator variable γ_i to represent the measurements from which source number. The total number of relative source is the sum of all sources found in each rotation: $\hat{N}'_s = \sum_{R=1}^{N_R} \hat{N}_{s,R}$. The numbering of each relative source has to be unique, $\gamma'_i = k'_{R_i} + k$, where $k'_R = \sum_{R'=1}^{R-1} \hat{N}_{s,R'}$ is the rotation offset. The parameters associated with the estimation of the relative source is displayed in Table. To estimates the unknown parameters, we set up a likelihood function and use the maximum of the likelihood function. The measurement function is given by :

$$h_i(c, p_k) = \frac{1}{c} \|\mathbf{p}_{d,s_i} - \mathbf{p}_k\| \tag{3.15}$$

The residue of the i^{th} measurement caused by the k^{th} source is $r_i(c, p_k) = h_i(c, p_k) - z_i$. Hence marginalized likelihood function is given as:

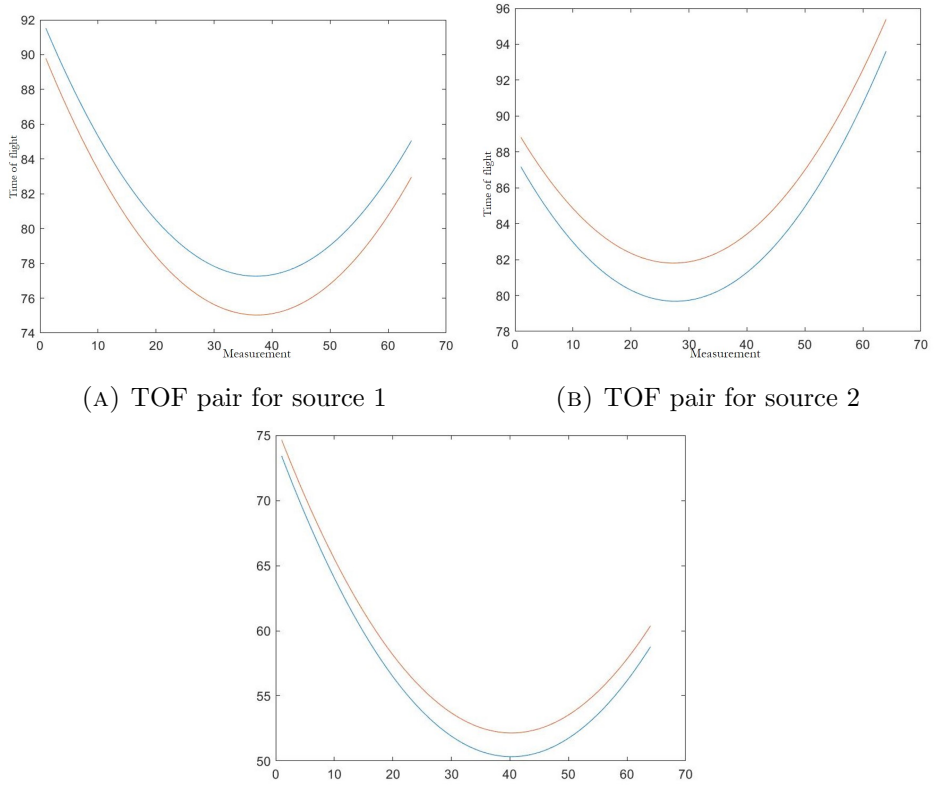

(A) TOF pair for source 1

(B) TOF pair for source 2

(C) TOF pair for source 3

FIGURE 3.5: Pairwise clustering of time of flight in a combined projection. Each figure represents the time of flight data for each source from different projections. Blue color represents the first projection and orange represents the second projection.

$$p(z_i|\ c, P') = \frac{1}{(N_s+1)\sqrt{2\pi}\sigma_z}\left(\sum_{k\in S_{R_i}} e^{-\frac{1}{2}\frac{r_i^2(c,p'_{s,k})}{\sigma_z^2}} + \frac{\sqrt{2\pi}\sigma_z}{v}\right) \tag{3.16}$$

Where the set $S_R = \{k'_R + 1, \ldots, k'_R + \hat{N}_{s,R}\}$ is the source number for every projection. To maximize the likelihood, we used an algorithm called the Expectation-Maximisation (EM) algorithm[Moon 96]. For the E-step of the algorithm, an initial guess of the both parameters is required, and it is calculating using the polynomial source parameters χ from the previous step. So the likelihood function will be $p(\gamma|z, \chi)$ instead of $p(\gamma|z, \hat{c}, \hat{P})$ only for the initial guess of the parameters.To start the algorithm, we will estimate the initial guess using the polynomial parameters:

$$(\hat{c}^{(1)}, \hat{P}^{(1)}) = \underset{c,P}{\operatorname{argmax}}\, E_{\gamma|z,\hat{\chi}}\,[log[p(z, \gamma|c, P)]] \tag{3.17}$$

Once we estimated the initial guess, the algorithm follows EM steps. For the E-step

$$(\hat{c}^{(j+1)}, \hat{P}^{(j+1)}) = \underset{c,P}{\operatorname{argmin}}\, Q(c, P, \hat{c}^{(j)}, \hat{P}^{(j)}) \tag{3.18}$$

The cost function is calculated by:

$$Q(c, P, \hat{c}, \hat{P}) = \sum_{i=1}^{N} \sum_{k=1}^{\hat{N}_s} r_i^2(c, p_k) w_{i,k}(\hat{c}, \hat{P}) \tag{3.19}$$

Where weight w is given in Equation 3.20 and it is depends on the rotation step. [Willemink 10]

$$w_{i,k}(\hat{c}, \hat{P}) = \frac{e^{-\frac{1}{2}\frac{r_i^2(\hat{c}, \hat{p}_k)}{\sigma_z^2}}}{\sum_{k'=1}^{\hat{N}_s} e^{-\frac{1}{2}\frac{r_i^2(\hat{c}, \hat{\mathbf{p}}_{k'})}{\sigma_z^2}} + \frac{\sqrt{2\pi}\sigma_z}{v}} \tag{3.20}$$

The M-step fits the model for unknown parameters. For that, we used the Gauss-Newton optimization [Guillaume 96]. Even though both parameters are unknown, we had no clue about the minimum.To solve this problem we used the Gauss-Newton method. The residue matrix of shape $N \times N_s$ residues and the residue vector is $r'(x) = (r'_1(c, \mathbf{p}_{s,1}), \ldots, r'_{\hat{N}_s}(c, \mathbf{p}_{s,\hat{N}_s}))$ .So the Jacobian matrix of the residue function will be:

$$\mathbf{H}_{c,k}^{(l)} = \begin{bmatrix} \frac{\partial}{\partial c} h_{1,k}^{(l)} \sqrt{w_{1,k}} \\ \vdots \\ \frac{\partial}{\partial c} h_{N,k}^{(l)} \sqrt{w_{N,k}} \end{bmatrix} \quad \mathbf{H}_{p_k}^{(l)} = \begin{bmatrix} \left(\frac{\partial}{\partial p_{s,k}} h_{1,k}^{(l)}\right)^T \sqrt{w_{1,k}} \\ \vdots \\ \left(\frac{\partial}{\partial p_{s,k}} h_{N,k}^{(l)}\right)^T \sqrt{w_{N,k}} \end{bmatrix}$$
$$\mathbf{H}^{(l)} = \begin{bmatrix} \mathbf{H}_{c,1}^{(l)} & \mathbf{H}_{p_1}^{(l)} & \\ \vdots & & \ddots \\ \mathbf{H}_{c,\hat{N}_s}^{(l)} & & & \mathbf{H}_{p_{\hat{N}_s}}^{(l)} \end{bmatrix} \tag{3.21}$$

as provided by [Willemink 10].The partial derivatives are given as:

$$\frac{\partial}{\partial c} h_{i,k}^{(l)} = \frac{-1}{c^{(l)}} h_i\left(c^{(l)}, \mathbf{p}_{s,k}^{(l)}\right) \tag{3.22}$$

$$\frac{\partial}{\partial \mathbf{p}_{s,k}} h_{i,k}^{(l)} = \left(\mathbf{p}_{s,k}^{(l)} - \mathbf{p}_{d,s_i}\right) \frac{1}{(c^{(l)})^2 h_i\left(c^{(l)}, \mathbf{p}_{s,k}^{(l)}\right)} \tag{3.23}$$

The iterative steps of the Gauss-Newton method for the optimization is :

$$\hat{\mathbf{x}}^{(l+1)} = \hat{\mathbf{x}}^{(l)} - \left(\mathbf{H}^{(l)T}\mathbf{H}^{(l)}\right)^{-1}\mathbf{H}^{(l)T} r'(\hat{\mathbf{x}}^{(l)}) \tag{3.24}$$

An example of applying relative source position algorithm is shown in the figure Figure 3.7. The expected and calculated relative source position displayed in the Figure 3.6.

The accuracy of the estimated parameters can be found using the covariance matrix, which is shown in the Equation 3.25

$$\hat{\mathbf{P}}_{\mathbf{xx}} = \mathbf{AWW^T A^T} \sigma_{\mathbf{w}}^{\mathbf{2}} \tag{3.25}$$

Where $\mathbf{A} = \left(\mathbf{H}^{(l)T}\mathbf{H}^{(l)}\right)^{-1}\mathbf{H}^{(l)T}$ and $\mathbf{W}$ is given as :

$$\mathbf{W} = \begin{bmatrix} diag\left(\sqrt{w_{1,1}}, \ldots, \sqrt{w_{N,1}}\right) \\ \vdots \\ diag\left(\sqrt{w_{1,\hat{N}_s}}, \ldots, \sqrt{w_{N,\hat{N}_s}}\right) \end{bmatrix} \tag{3.26}$$

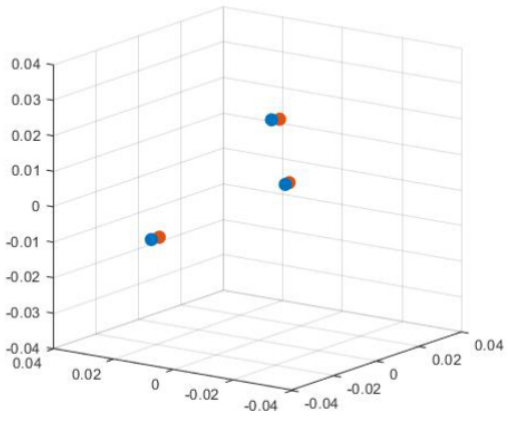

(A) Combined Projection 1

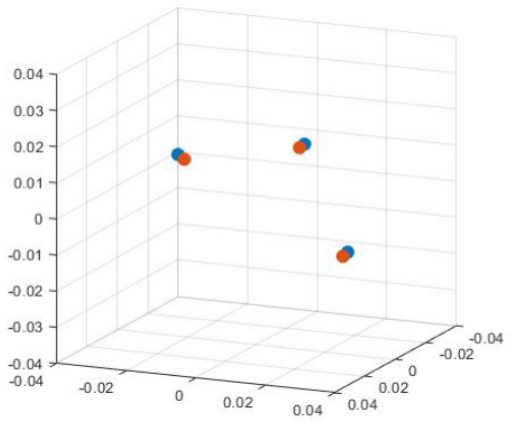

(B) Combined Projection 2

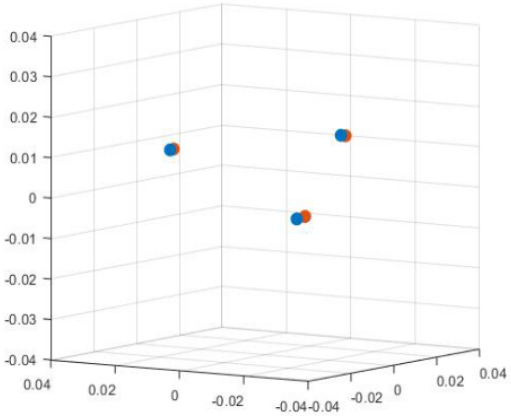

(C) Combined Projection 3

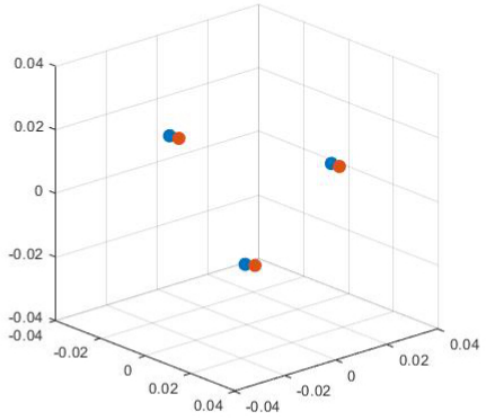

(D) Combined Projection 4

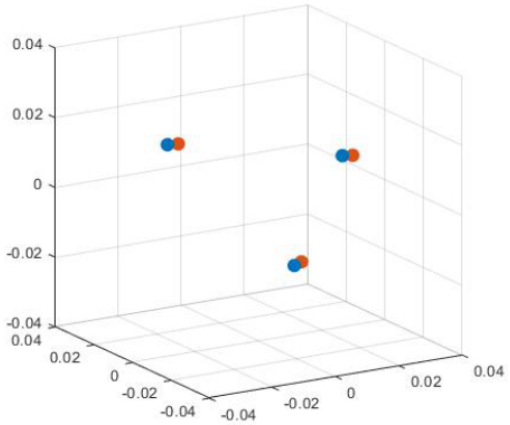

(E) Combined Projection 5

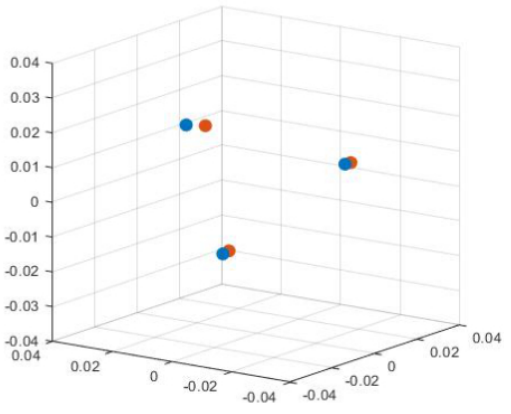

(F) Combined Projection 6

FIGURE 3.6: Expected and calculated relative source position. Blue color is the expected source position and the red color is the calculated source position.

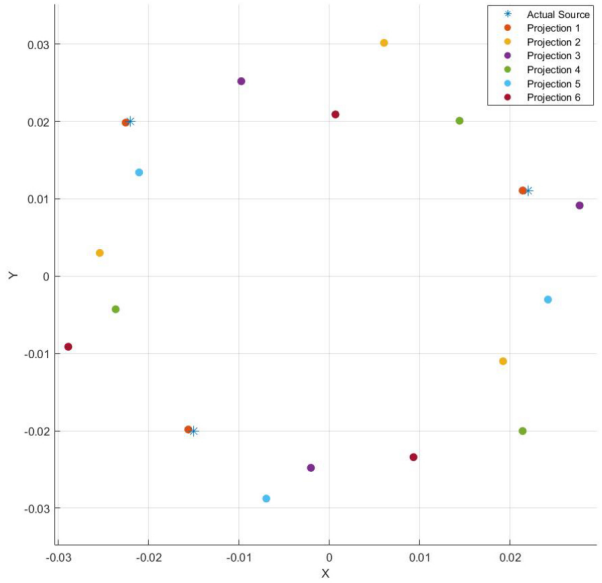

(A) Relative source position from top view

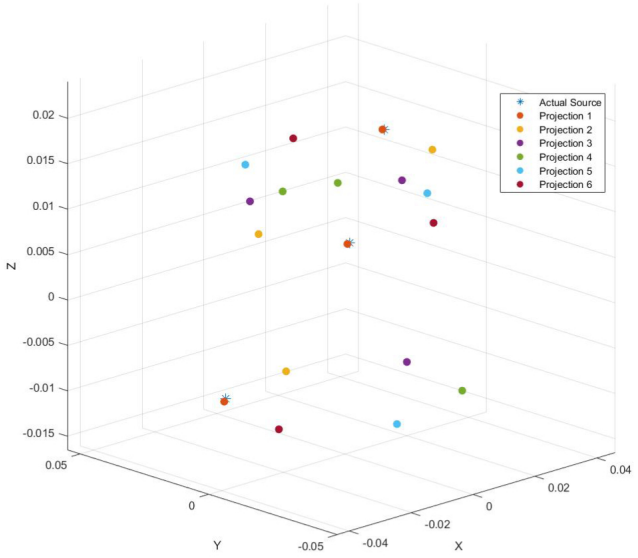

(B) Relative source position from side view

FIGURE 3.7: An example of relative source position plotted all projections together

3.4 Estimation of center of rotation

From the previous step, calculated the speed of ultrasound and a group of source positions from different projections and a covariance matrix with the uncertainty of the parameters. First, associate in nursing initial guess of the source position and

center of rotation will estimate and so the ultimate estimate of the all the parameters using the complete likelihood function.

Initial guess

Initial guess of the center of rotation, absolute source position, and the number of sources are the parameters we are estimating using the previous step results. The number of sources in the calibration needs to determine because all sources are not necessary to visible in every rotation. We start by grouping the relative source position as pairs from different rotations, and it is given by $S_p = \{(k_1 \in S_{R_1}, (k_2 \in S_{R_2}) : R_1 \neq R_2\}$. Let's consider two relative source positions belongs to different projections . We could find the center of rotation and source position from this pair if they are from same point source. Relation between relative and absolute source position and center of rotation is $\mathbf{p}'_{s,k_1} = R_{\phi R_1}\mathbf{p}_{s,k} + \mathbf{T}$. If we could get a pair from different rotation steps, then the relationship between the parameters is shown in the Equation 3.27, and inverting the equation can estimate the unknown parameters given in Equation 3.28.Where the R is the rotation matrix given in Equation 3.29, and I is the identity matrix.

$$\begin{bmatrix} \mathbf{p}'_{s,k_1} \\ \mathbf{p}'_{s,k_1} \end{bmatrix} = \mathbf{A} \begin{bmatrix} \mathbf{p}_{s,k} \\ \mathbf{T} \end{bmatrix} \quad \text{where} \quad \mathbf{A} = \begin{bmatrix} \mathbf{R}_{\phi R_1} & \mathbf{I} \\ \mathbf{R}_{\phi R_1} & \mathbf{I} \end{bmatrix} \tag{3.27}$$

$$\begin{bmatrix} \mathbf{p}_{s,k} \\ \mathbf{T} \end{bmatrix} = \mathbf{A}^{-1} \begin{bmatrix} \mathbf{p}'_{s,k_1} \\ \mathbf{p}'_{s,k_1} \end{bmatrix} \tag{3.28}$$

$$\mathbf{R} = \begin{bmatrix} cos(\phi) & -sin(\phi) & 0 \\ sin(\phi) & cos(\phi) & 0 \\ 0 & 0 & 1 \end{bmatrix} \tag{3.29}$$

We can decompose matrix $\mathbf{A}^{-1}$ as $\begin{bmatrix} \mathbf{A}_p \\ \mathbf{A}_T \end{bmatrix}$. In the previous step, we calculated the covariance matrix $\hat{\mathbf{P}}_{\mathbf{xx}}$, and here we can use it to calculate the uncertainty of the calibration parameters. If the pair $\mathbf{S}_p$ contains $(\mathbf{p}_{s,k_1}, \mathbf{p}_{s,k_2})$, then we extract the portion of the $\hat{\mathbf{P}}_{\mathbf{xx}}$ matrix associated to the pair gives a 6×6 matrix $\mathbf{P}_{k_1,k_2}$. Then the uncertainty of the center of rotation is given by:

$$\mathbf{P}_T = \mathbf{A}_T \mathbf{P}_{k_1,k_2} \mathbf{A}_{\mathbf{T}}^T \tag{3.30}$$

Then we can calculate the squared Mahalanobis distance of all the pairs using the $d_p^2(\mathbf{T}) = \left(\hat{\mathbf{T}}_p - \mathbf{T}\right)^T \mathbf{P}_{T_p}^{-1} \left(\hat{\mathbf{T}}_p - \hat{\mathbf{T}}\right)$, and using the cumulative distribution function, we could calculate a score $c_p = 1 - F_{\chi_3^2}(d_p^2)$ between 0 and 1. If the score is higher, the calculated center of rotations are close to the actual center of rotation[Willemink 10]. The algorithm for center of rotation and source position is displayed in figure as pseudo-code.

Optimizing the complete likelihood function

In order to estimate the calibration parameters, we have to optimise the whole likelihood function $p(\mathbf{z}|c, \mathbf{T}, P)$. From the previous step, we calculated an initial estimation of all the parameters. The complete measurement function is:

$$h_i c, \mathbf{T}, \mathbf{p}_{s,k} = \frac{1}{c} \|\mathbf{p}_{d,s_i} - \mathbf{R}_{\phi,s_i} \mathbf{p}_{s,k} - \mathbf{T}\| \tag{3.31}$$

The complete likelihood function for the measurement z_i is:

$$p(\mathbf{z}|c, \mathbf{T}, P) = \frac{1}{(\hat{N}_s + 1)\sqrt{2\pi}\sigma_z} \left(\sum_{k=1}^{\hat{N}_s} e^{-\frac{1}{2} \frac{r_i^2(c, \mathbf{T}, \mathbf{p}_{s,k})}{\sigma_z^2}} + \frac{\sqrt{2\pi}\sigma_z}{v} \right) \tag{3.32}$$

To maximize the likelihood, we used the same EM algorithm, which we used earlier. The cost function associated with the optimization is given as:

$$Q(c, \mathbf{T}, P, \hat{c}, \hat{\mathbf{T}}, \hat{P}) = \sum_{i=1}^{N} \sum_{k=1}^{\hat{N}_s} r_i^2(c, \mathbf{T}, \mathbf{p}_{s,k}) w_{i,k}(\hat{c}, \hat{\mathbf{T}}, \hat{P}) \tag{3.33}$$

where the weight function is:

$$w_{i,k}(\hat{c}, \hat{\mathbf{T}}, \hat{P}) = \frac{e^{-\frac{1}{2} \frac{r_i^2(\hat{c}, \hat{\mathbf{T}}, \hat{p}_k)}{\sigma_z^2}}}{\sum_{k'=1}^{\hat{N}_s} e^{-\frac{1}{2} \frac{r_i^2(\hat{c}, \hat{\mathbf{T}}, \hat{\mathbf{p}}_{k'})}{\sigma_z^2}} + \frac{\sqrt{2\pi}\sigma_z}{v}} \tag{3.34}$$

The calculated and expected center of rotation is given in figure Figure 3.8

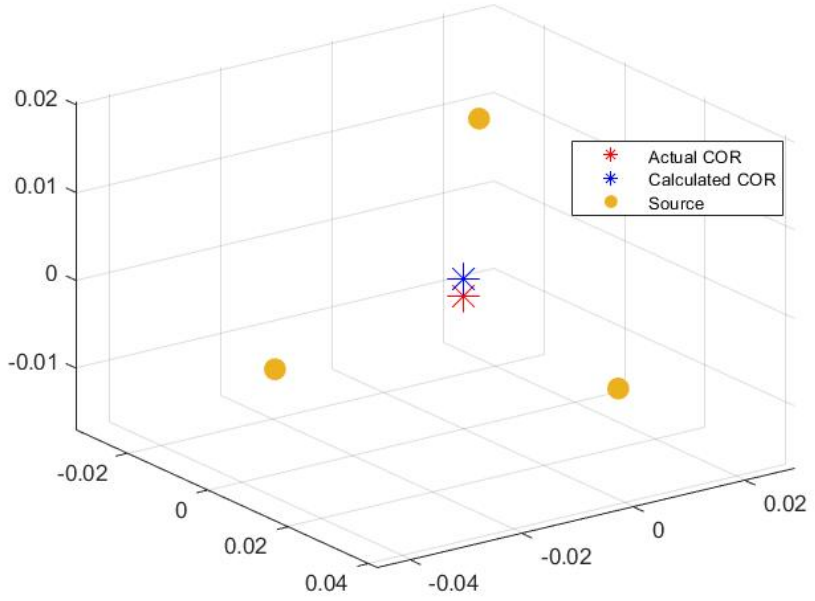

FIGURE 3.8: An example of expected and calculated center of rotation(COR).

3.5 Conclusion

This chapter included the calibration algorithm of three-dimensional photoacoustic tomography using the time of flight data. Ultrasound time of flight data generated by the Matlab toolbox 'k-wave.' Interested calibration parameters are the COR, SOS and source position. The algorithm automatically estimates the number of point sources and outliers. The algorithm's accuracy increases with the number of point sources and the number of projections. But the time of flight grouping algorithm shows errors when the source number is higher. The relative source position is challenging to estimate using a single projection, and so we combined two projections.

Chapter 4

Experimental Implementation

4.1 Mechanical design of the rotatory stage

In the calibration setup, the linear transducer rotates around the calibration object shown in shown in Figure 2.3c. We had to design a setup where we can attach the calibration object at the center, and the sensor can rotate around it. So we designed the set up in Solid Works is shown below.

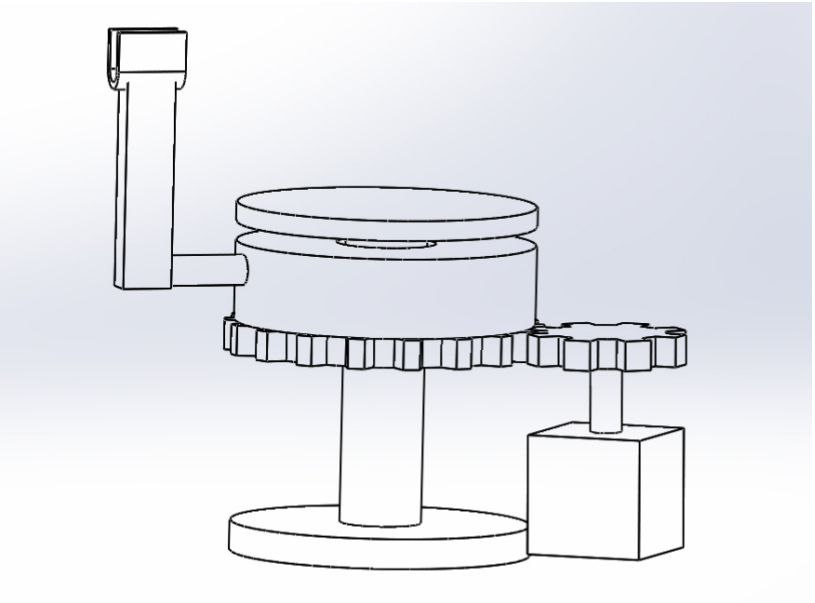

FIGURE 4.1: Rotatory stage designed using solidworks

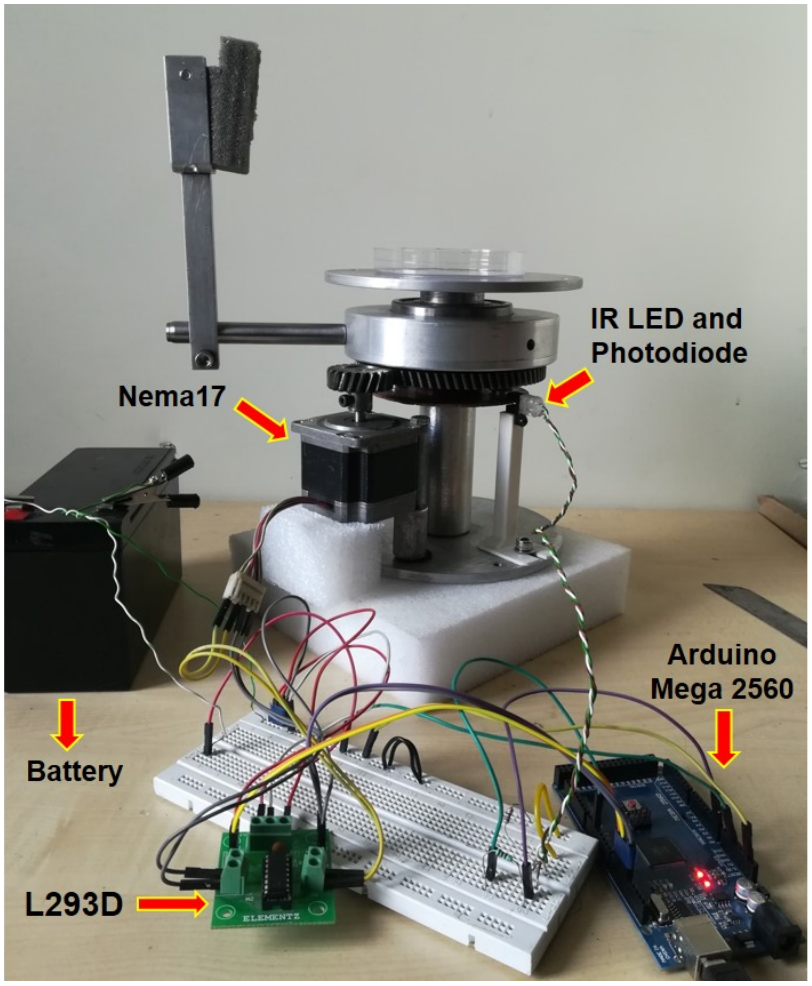

(A) Mechanical design of the rotatory stage.

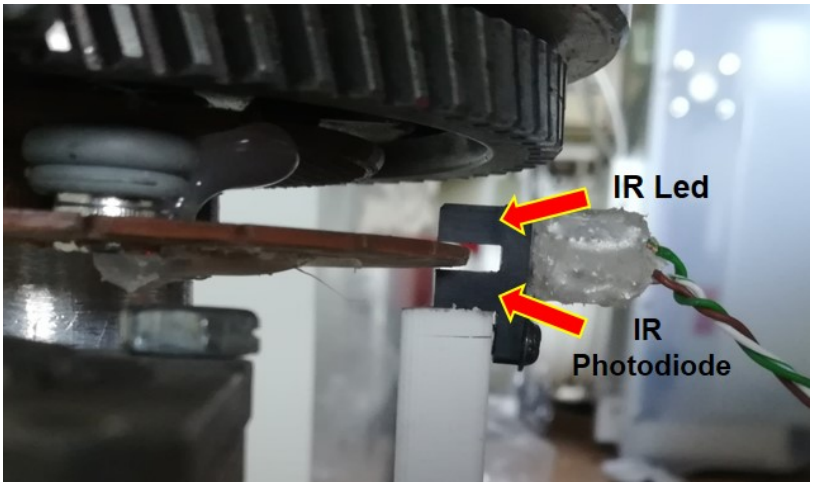

(B) IR led and photodiode setup for the rotation control

FIGURE 4.2: Mechanical setup for calibration measurements. The rotation of the motor is controlled using LM293D and arduino mega. The IR led-photodiode used for accurate projections.

For the rotation of the detector array, we used NEMA-17 stepper motor, Arduino Mega microcontroller, and L293D motor driver for controlling the rotation of the detector array. Each part of the setup and the circuit is shown in the Figure 4.2a.To control the rotation step, we used an IR led and a photodiode for better accuracy is shown in the Figure 4.2b. Along with the photodiode and led, we 3D printed a rotatory plate is shown in figure. We integrated this setup with the microcontroller and controlled rotation of the stepper motor according to the calibration setup. The arduino code written for the setup is given in Appendix A.

4.2 Testing the detection of ultrasound

For the experimental part, we made tissue-mimicking phantom with number of point sources. We used human hair with a length of $0.2mm$ in 2% of agar as a calibration object[Souza 16]. To check the detection of the ultrasound, we placed three hairs at the center of the calibration tube with a spacing less than $1cm$ is shown in Figure 4.3.

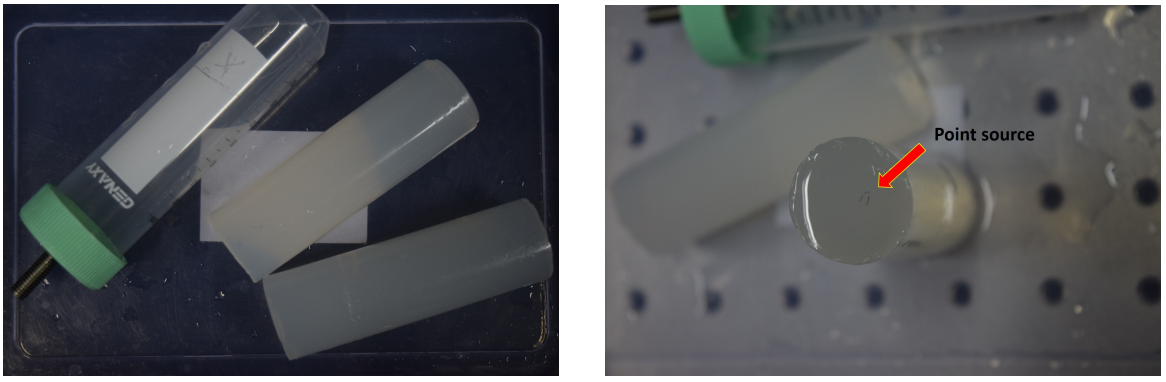

(A) Phantom and phantom tube (B) Phantom with points sources

FIGURE 4.3: Calibration phantom with point sources

We used $690nm$ wavelength red laser as an illumination source. To achieve the acoustic coupling, we immersed the calibration phantom and the transducer in the water.The reconstructed image of the point source is shown in Figure 4.4b.

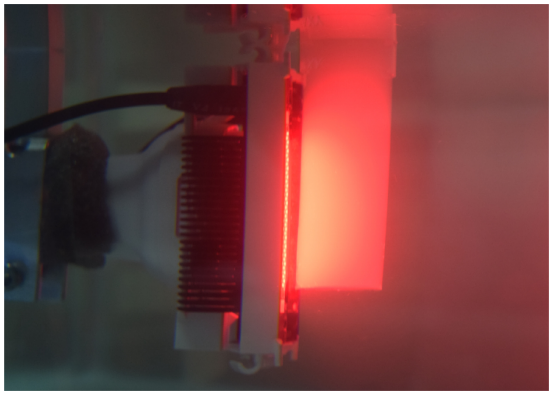

(A) Linear transducer,laser and phantom

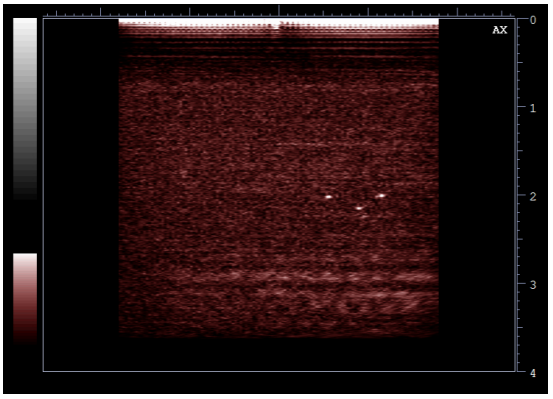

(B) Reconstructed image of point sources

FIGURE 4.4: Detection of ultrasound: Setup and reconstructed image

The experimental calibration setup is shown in Figure 4.5.

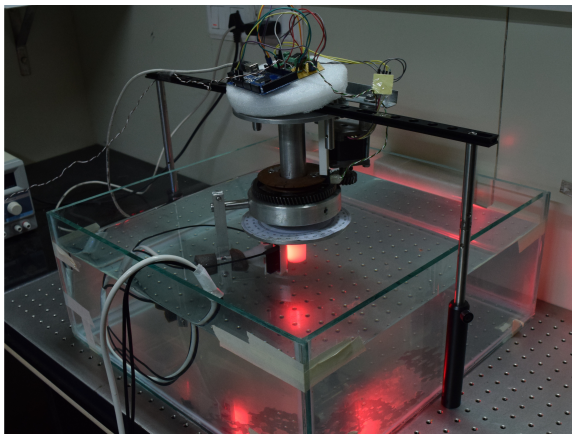

(A) Total calibration setup

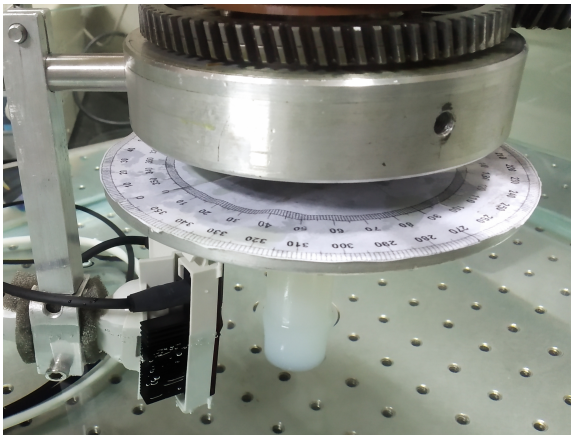

(B) Phantom and ultrasound transducer on rotatory stage

FIGURE 4.5: Experimental setup for the calibration

4.3 Results and conclusion

In this chapter, we have done the experimental implementation of the calibration. We used agar phantom as calibration object and hair as point source. The reconstructed image of the three point sources and the corresponding ultrasound signals is shown in Figure 4.6.

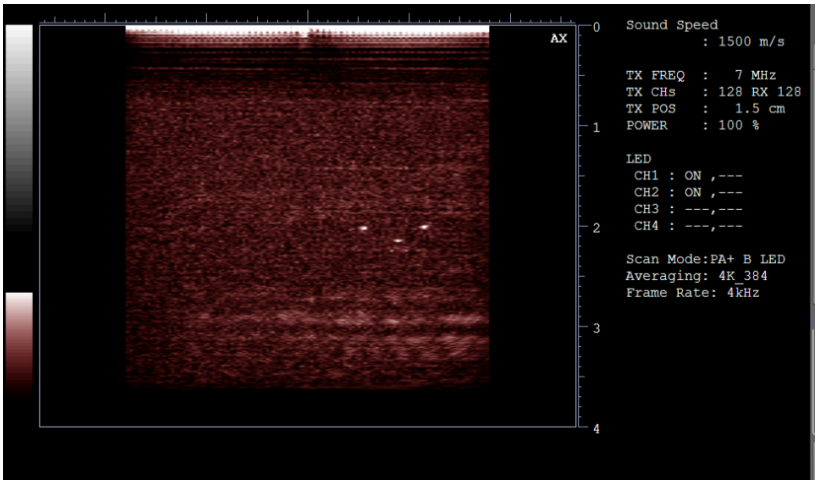

(A) Reconstructed image of the three point sources

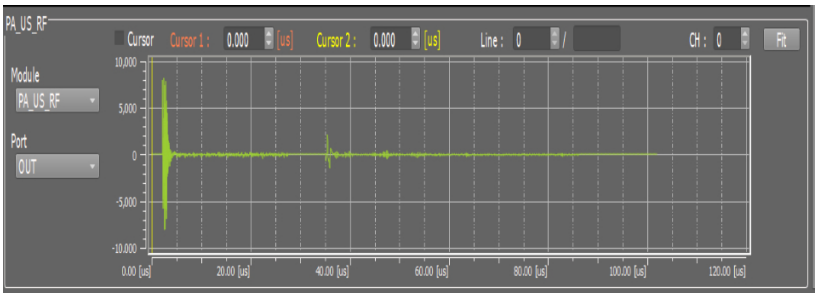

(B) Recorded ultrasound signals

FIGURE 4.6: Reconstructed image and ultrasound signals of the point sources

Future works

According to the calibration algorithm, we need the time of flight data of all sources in each projection. The ultrasound transducer rotates around the stationary calibration object, and it gets the time of flight data. We faced a problem in getting the ultrasound signals for all the sources in a single projection. It might be because of the less acceptance angle of the linear transducer we used. We could solve it by making the point sources closer and placing the transducer in the proper place. Also, we could introduce more laser sources for strong ultrasound signals. We have used agar phantom and hair as point sources, but it is not spherically symmetric so that the size may vary in different projections. We have to replace the point sources to spherical sources so that we could maintain the same size in all the projections. As an initial step, we manually controlled the rotation using a stepper motor and photoacoustic machine for recording the time of flight in each projection. We could make a trigger for controlling the photoacoustic machine using the IR led and photodiode setup.

The accuracy of the calibration algorithm increases with number of point sources and projections. So we could increase the number of sources and more projections.

Appendix A

Arduino programming to control the stepper motor

This is the arduino program to control the stepper motor using the IR led and photodiode.

```
1      /// Stepper Motor
2 #include <Stepper.h>
3 const int stepsPerRevolution = 200;
4 /// IR Sensor
5  int timedelay = 15000; /Delay for each projection
6  int pd = 2;
7  int count=0;
8  int senRead=0;
9  int limit=850;
10  int skip=2;
11
12  int stopcount=0;
13 Stepper myStepper(stepsPerRevolution,9,10,11,12);
14
15 void setup()
16 {
17   myStepper.setSpeed(10);  // stpper motor speed
18   pinMode(pd,OUTPUT);
```

```
19   digitalWrite(pd,HIGH);
20   Serial.begin(9600);
21 }
22
23
24 void loop()
25  {
26
27 if (analogRead(senRead) < limit) { //
28   if (count == 0 || count == 1){
29     delay(timedelay);
30   }
31   count = (count+1)%(skip+2);
32   stopcount = stopcount + 1 ;
33   Serial.println(stopcount);
34   if (stopcount==24){
35   for(;;){}
36   }
37   while(1) {
38     myStepper.step(1);
39     if (analogRead(senRead) > limit)
40       break;
41   }
42 }
43 else
44   myStepper.step(1);
45  }
```

Bibliography

[Fischler 81] Martin A. Fischler & Robert C. Bolles. *Random Sample Consensus: A Paradigm for Model Fitting with Applications to Image Analysis and Automated Cartography.* Commun. ACM, vol. 24, no. 6, page 381–395, June 1981.

[Fletcher 13] Roger Fletcher. Practical methods of optimization. John Wiley & Sons, 2013.

[Francis 16] KJ Francis, Pradeep Mishra, Pachamuthu Rajalakshmi, Sumohana S Channappayya & Ashutosh Richhariya. *A simple and accurate matrix for model based photoacoustic imaging.* In 2016 IEEE 18th International Conference on e-Health Networking, Applications and Services (Healthcom), pages 1–5. IEEE, 2016.

[Guillaume 96] P. Guillaume & R. Pintelon. *A Gauss-Newton-like optimization algorithm for "weighted" nonlinear least-squares problems.* IEEE Transactions on Signal Processing, vol. 44, no. 9, pages 2222–2228, 1996.

[Hoelen 98] C. G. A. Hoelen, F. F. M. de Mul, R. Pongers & A. Dekker. *Three-dimensional photoacoustic imaging of blood vessels in tissue.* Opt. Lett., vol. 23, no. 8, pages 648–650, Apr 1998.

[Kolkman 08] Roy G. M. Kolkman, Peter J. Brands, Wiendelt Steenbergen & Ton G. C. van Leeuwen. *Real-time in vivo photoacoustic and ultrasound imaging.* Journal of Biomedical Optics, vol. 13, no. 5, pages 1 – 3, 2008.

[Kostli 01] KP Kostli, Daniel Frauchiger, Joël J Niederhauser, Günther Paltauf, Heinz P Weber & Martin Frenz. *Optoacoustic imaging using*

a three-dimensional reconstruction algorithm. IEEE Journal of Selected Topics in Quantum Electronics, vol. 7, no. 6, pages 918–923, 2001.

[Köstli 03] Kornel P Köstli & Paul C Beard. *Two-dimensional photoacoustic imaging by use of Fourier-transform image reconstruction and a detector with an anisotropic response.* Applied optics, vol. 42, no. 10, pages 1899–1908, 2003.

[Kruger 95] Robert A Kruger, Pingyu Liu, Yuncai "Richard" Fang & C Robert Appledorn. *Photoacoustic ultrasound (PAUS)—reconstruction tomography.* Medical physics, vol. 22, no. 10, pages 1605–1609, 1995.

[Ku 01] Geng Ku & Lihong V Wang. *Scanning microwave-induced thermoacoustic tomography: Signal, resolution, and contrast.* Medical physics, vol. 28, no. 1, pages 4–10, 2001.

[Ku 04] Geng Ku, Xueding Wang, George Stoica & Lihong V Wang. *Multiple-bandwidth photoacoustic tomography.* Physics in Medicine & Biology, vol. 49, no. 7, page 1329, 2004.

[Manohar 04] Srirang Manohar, Alexei Kharine, Johan C. G. van Hespen, Wiendelt Steenbergen & Ton G. van Leeuwen. *Photoacoustic mammography laboratory prototype: imaging of breast tissue phantoms.* Journal of Biomedical Optics, vol. 9, no. 6, page 1172, January 2004.

[McLachlan 88] Geoffrey J McLachlan & Kaye E Basford. Mixture models: Inference and applications to clustering, volume 38. M. Dekker New York, 1988.

[Minghua Xu 02] Minghua Xu & L. V. Wang. *Time-domain reconstruction for thermoacoustic tomography in a spherical geometry.* IEEE Transactions on Medical Imaging, vol. 21, no. 7, pages 814–822, 2002.

[Moon 96] T. K. Moon. *The expectation-maximization algorithm.* IEEE Signal Processing Magazine, vol. 13, no. 6, pages 47–60, 1996.

[Souza 16] Rebeca Monteiro Souza, Taynara Queiroz Santos, Débora Paulino Oliveira, AV Alvarenga & RPB Costa-Felix. *Standard operating*

procedure to prepare agar phantoms. In Journal of Physics: Conference Series, volume 733, page 012044. IOP Publishing, 2016.

[Treeby 10] Bradley E Treeby & Benjamin T Cox. *k-Wave: MATLAB toolbox for the simulation and reconstruction of photoacoustic wave fields.* Journal of biomedical optics, vol. 15, no. 2, page 021314, 2010.

[Vaithilingam 09] S. Vaithilingam, T. Ma, Y. Furukawa, I. O. Wygant, X. Zhuang, A. De La Zerda, O. Oralkan, A. Kamaya, S. s. Gambhir, R. B. Jeffrey & B. T. Khuri-yakub. *Three-dimensional photoacoustic imaging using a two-dimensional CMUT array.* IEEE Transactions on Ultrasonics, Ferroelectrics, and Frequency Control, vol. 56, no. 11, pages 2411–2419, 2009.

[Wang 08] Lihong V Wang. *Tutorial on photoacoustic microscopy and computed tomography.* IEEE Journal of Selected Topics in Quantum Electronics, vol. 14, no. 1, pages 171–179, 2008.

[Wang 12] Lihong V Wang & Hsin-i Wu. Biomedical optics: principles and imaging. John Wiley & Sons, 2012.

[Willemink 10] Rene Willemink. *Image reconstruction in a passive element enriched photoacoustic tomography setup.* PhD thesis, University of Twente, Netherlands, 6 2010. eemcs-eprint-18529.

[Xu 02] Minghua Xu & Lihong V Wang. *Time-domain reconstruction for thermoacoustic tomography in a spherical geometry.* IEEE transactions on medical imaging, vol. 21, no. 7, pages 814–822, 2002.

[Xu 06] Minghua Xu & Lihong V. Wang. *Photoacoustic imaging in biomedicine.* Review of Scientific Instruments, vol. 77, no. 4, page 041101, 2006.

[Zemp 07] Roger J. Zemp, Rachel Bitton, K. Kirk Shung, Meng-Lin Li, George Stoica D.V.M. & Lihong V. Wang. *Photoacoustic imaging of the microvasculature with a high-frequency ultrasound array transducer.* Journal of Biomedical Optics, vol. 12, no. 1, pages 1 – 3, 2007.